RSC Advances

ROYAL SOCIETY OF CHEMISTRY

www.rsc.org/advances

High-quality ZnO nanorods based flexible devices for electronic and biological applications

N. Koteeswara Reddy,[1,2*,#] M. Devika,[1,3] C. W. Tu[1,4*]

[1]Department of Nanobio Materials and Electronics, Gwangju Institute of Science and Technology, Gwangju 500712, Korea

[2]Center for Nanoscience and Engineering, Indian Institute of Science, Bangalore 560012, India

[3]Department of Aerospace Engineering, Indian Institute of Science, Bangalore 560012, India

[4]Department of Electrical and Computer Engineering, University of California, San Diego, La Jolla, California 92093-0407, USA

Vertically aligned zinc oxide nanorods (ZnO NRs) were synthesized on kapton flexible sheets using a simple and cost-effective three-step process (electrochemical seeding, annealing under air ambient, and chemical solution growth). Scanning electron microscopy studies reveal that ZnO NRs grown on seed-layers, developed by electrochemical deposition at a negative potential of 1.5 V in the duration of 2.5 min and annealed at 200 ^{o}C for 2 h, consist of uniform morphology and good chemical stoichiometry. Transmission electron microscopy analyses show that the as-grown ZnO NRs have single crystalline hexagonal structure with a preferential growth direction of <001>. Highly flexible p-n junction diodes fabricated by using p-type conductive polymer exhibited excellent diode characteristics even under fold state.

*Corresponding authors: (NKR) E-mail: dr_nkreddy@rediffmail.com and (CWT) E-mail: ctu@soe.ucsd.edu, #Present address: Institute of Chemistry, Humboldt University, 12489 Berlin, Germany, Tel: +49-30-2093-7441.

1. Introduction

Vertically aligned zinc oxide (ZnO) nanorod structures (NRs) have great potential applications in various fields including lasers, sensors, solar cells, and space engineering.[1-3] Further, ZnO NRs are expected as appropriate candidates for bio imaging, detection of extra- and intra- cellular metallic ions, and biological species.[4-7] ZnO is a wide band gap semiconductor material (3.35 eV) and usually consists of higher exciton binding energy (60 meV), which is 2.3 times higher than the energy available at room temperature.[8] Generally, it exhibits wurtzite hexagonal crystal structures, and n-type electrical conductivity. So far, there have been a large number of publications on the development of ZnO nanostructures and devices.[9-13] In most cases, the adopted substrates are rigid materials. However, the development of flexible devices for different scientific applications has received great attention due to their significant advantages over rigid ones including light weight, durability, and low-cost.[14] On the other hand, it is also possible to develop efficient and physiological friendly bio devices for drug-delivery, detection of different elements, and biological analytes.[15]

Considerably most of the techniques and/or methodologies used for the development of active structures on flexible substrates are expensive, hectic, and time consuming.[16-24] For example, vertically grown ZnO NRs on indium tin oxide/polyethylene terephthalate (ITO/PET) substrates were developed and adopted in the fabrication of dye sensitized solar cell (DSSC) devices.[25] Though the observed photo conversion efficiency of the DSSC device is quite good (3.15%), the adopted methods such as laser interference lithography for pattering, sputtering for deposition of Zn metal, transfer of Zn metals on to the ITO/PET substrate are expensive, difficult

for large scale production, and even reproducibility is also poor. On the other hand, Lee et al. have observed good saturation mobility (7.5 cm^2 $V^{-1}s^{-1}$) and high drain current on-to-off ratio (10^4) from ZnO thin films based transistors.[26] Zainelabdin et al. have developed flexible white light emitting diodes using vertically aligned ZnO NRs and observed good stability with respect to temperature.[20] Similarly, Hyuck Lee et al. have developed flexible inverted organic solar cell devices and observed three-fold increase in photo conversion efficiency.[21] In all these approaches, the active ZnO seed layers are developed by spin coating of zinc precursor solution followed by annealing. Here, the adhesion between the seed layer and substrate is poor due to the nominal attachment of active particles (nuclei sites) to the substrate with weak attractive forces, which strongly affects the growth of nanorods and thereby the device performance.

To overcome the above difficulties, a simple and cost effective methodology has been developed and adopted for the fabrication of highly flexible devices. Basically this methodology consists of three-steps: seeding, annealing, and growth of nanostructures (named as SAG method), which is scalable and also short-time process. Preliminary results obtained by using SAG method have been reported elsewhere.[27] In this article, we report the synthesis of high quality ZnO NRs on flexible substrates using SAG method by optimizing the ZnO seed-layer deposition parameters. Further, vertically aligned ZnO NRs based p-n junction devices were fabricated and studied their diode performance under normal as well as fold condition.

2. Experimental procedure:

The experimental procedure of ZnO NRs growth on flexible substrates using SAG method, fabrication of highly flexible devices, and characterization techniques are briefly described in the following sections.

2.1. Growth of ZnO NRs:

Vertically aligned ZnO NRs were grown on flexible substrates by using SAG procedure.[27] In brief, initially ZnO seed-layer was deposited by electrochemical deposition on nickel coated kapton sheets and annealed in air ambient. Finally, the ZnO NRs structures were grown by chemical solution method at a growth temperature of 70 ^{o}C in the reaction time of 6 h. Here, the bath solution was prepared using zinc nitrate hexahydrate ($ZnO_6N_2.6H_2O$) and hexamethylenetetramine ($C_6H_{12}N_4$) (analytical grade chemicals from Sigma-Aldrich) with a concentration of 10 mM.

The impact of negative potential (V_c), deposition time (D_t), and annealing temperature (A_T) of seed-layers on the growth of vertically aligned ZnO NRs was studied and optimized. The ZnO seed-layers were deposited by electrochemical deposition on Ni (20 nm by e-beam evaporation) coated flexible substrates at different negative potentials of 0.5, 1.0, 1.5 and 2.0 V by keeping other conditions as constant (D_t = 1 min, A_T = 150 ^{o}C, and annealing time (A_t) = 2 h). Then, the seed-layer deposition time was varied from 30 s to 5 min by keeping the negative potential, A_T and A_t as constant at 1.5 V, 150 ^{o}C, and 2 h respectively. Finally, the seed-layers deposited at V_c = 1.5 V, D_t = 2.5 min, and A_t = 2 h were annealed at different temperature varied from 100 to 250 ^{o}C.

2.2. Fabrication of p-n junction device:

In order to maintain bottom contact, a small area of Ni/kapton was covered with adhesive tape and then, ZnO seeds were deposited on Ni/kapton substrates using electrochemical deposition under optimized conditions such as negative potential of 1.5 V for 2.5 min. Then, the structures were annealed at 200 ^{o}C for 2 h and used for the growth of vertically aligned ZnO NRs. Finally, a thick layer of poly(3,4-ethylene-di-oxy-thiophene) poly(styrene-sulfonate) (PEDOT:PSS) polymer was spin coated as a p-type layer and the configuration of final device was made as Au/PEDOT:PSS/ZnO NRs/ZnO seeds/Ni/flexible substrate.

2.3. Characterization:

The surface morphology, chemical composition, crystal structure, and emission properties of as-grown ZnO NRs were analyzed using field emission scanning electron microscopy (FESEM, Hitachi S-4700), transmission electron microscopy (TEM), selected area electron diffraction (SAED) microscopy, Energy dispersive X-ray spectroscopy (EDS) and cathodoluminescence (CL). The p-n junction device performance was studied at room temperature under flat and fold conditions using probe-station attached with semiconductor analyzer.

3. Results and discussion

3.1. ZnO NRs on flexible substrates:

FESEM analyses of ZnO NRs (Fig. 1) grown on the electrochemical deposited ZnO seed-layers reveal that the negative potential applied for the deposition of seed-layers has strong impact on the morphology of as-grown ZnO NRs. In particular, ZnO NRs grown on seed-layers deposited with a negative potential of 1.5 V consist of nearly uniform morphology (Fig. 1b) than the structures grown on seed layers

deposited at other potentials. The ZnO NRs grown on seed-layers that were developed at lower (Fig. 1a) as well as higher potentials (Fig. 1c and 1d) have uneven and zigzag morphologies. The change in morphology with deposition potential of seed-layers mainly attributed to rate of nucleation and thereby the formation of seed-layer.[28] At lower potentials (≤ 1.0 V), the nucleation of Zn and O atoms on Ni coated flexible substrates could be low and thus, it forms like a non-continuous film. At higher voltages (≥ 2.0 V), there could be an over growth at certain places due to high rate of nucleation, which leads the film surface to uneven. As a result, non-uniform morphology for ZnO NRs grown on seed-layers deposited at lower as well as higher potentials. On the other hand, the average diameter of the as-grown ZnO NRs increased with the increase of negative potential applied for the deposition of seed-layers.

The surface morphology of ZnO NRs grown on seed-layers deposited at a negative potential of 1.5 V in different reaction timings varied from 30 s to 5 min is shown in Fig 2. The structures grown on the seed-layers deposited in the duration of 2.5 min exhibited nearly smooth and uniform morphology than the structures grown on seed-layers deposited at other deposition timings. A poor morphology of ZnO NRs on the seed-layers deposited at lower reaction timings (≤ 2 min) can be clearly observed from Fig. 2a, which is probably attributed to the formation of ultra-thin non-uniform ZnO clusters (layer).[29] At higher reaction timings (≥ 3 min), the textured morphology of ZnO NRs is due to presence of over-growth or segregated particles on the surface of seed-layers. Details about the segregated ZnO seed-layer can be found from supporting information (SI-1). Therefore, the ZnO NRs grown on the seed-layers

deposited in the reaction time, $2 < D_t < 3$ min have considerably good surface morphology.

The ZnO NRs structures grown on annealed seed-layers exhibited different morphologies as shown in Fig. 3. While increasing the annealing temperature of seed-layers from 100 to 200 ^{o}C, the morphology of ZnO NRs gradually improved and becomes uniform. However, the morphology of ZnO NRs grown on seed-layers annealed at higher temperatures, > 200 ^{o}C, slightly degraded (Fig. 3d) and the growth also discontinuous. As compared to other structures, the ZnO NRs grown on seed-layers annealed at 200 ^{o}C consist of excellent uniform morphology and however, the average diameter of the ZnO NRs is found to be 82 nm. In general, while increasing the annealing temperature the quality as well as crystallinity of seed-layers increase, which probably leads the growth of ZnO NRs to more epitaxial and uniform. However, the degradation in the growth of ZnO NRs on the seed-layers annealed at high temperatures probably attributed to deformation of kapton substrate since it starts to melt at above 260 ^{o}C.

The crystal structure and optical properties of ZnO NRs grown on seed-layers prepared with a negative potential of 1.5 V in the duration of 2.5 min followed by annealing at 200 ^{o}C for 2 h were analyzed by TEM and CL. TEM, high resolution TEM (HRTEM) and SAED images of these NRs are shown in Fig. 4. TEM analysis shows that the diameter of ZnO NR is about 85 nm (Fig. 4a), which is consistent with FESEM measurements. HRTEM studies show that ZnO NRs are purely single crystalline and grown along <001> direction since the observed d-spacing value of the diffraction fringes is 0.263 nm (Fig. 4b). Further, the single crystallinity and growth

direction of ZnO NRs is confirmed by SAED (Fig. 4c). The phase purity and preferential orientation of these ZnO NRs, observed from X-ray diffractometer (XRD) studies (see SI-2), noticeably consistent with the above data. EDS analysis shows that the as-grown ZnO NRs have nearly stoichiometric chemical composition and exhibited the Zn and O atomic percent ratio of 1.05. CL studies (Fig. 4d) show that ZnO NRs consist of three emission peaks: sharp ultra-violet (UV) emission peak centered at 3.25 eV, broad band (BB) orange emission peak at around 2.1 eV and small red emission peak at 1.64 eV. The UV emission peak, represents the near band edge emission, arises from the recombination of exited carriers at valance band. On the other hand, the broad emission peak represents defects related emission, which probably arises from the recombination of exited carriers at different defects related energy states.[8, 30] On the other hand, a small and sharp red emission peak centered at 1.64 eV probably belongs to zinc interstitials (Zn_I).[31] Further, the intensity ratio between UV and BB peaks (I_{UV}/I_{BB}) i.e. figure of merit is about 6 and the full width at half maximum (FWHM) value of UV peak is found to be 145 meV. This indicates that ZnO NRs grown on seeded flexible substrates under optimized conditions have good crystallinity quality and chemical as well as phase purity.

3.2. Flexible devices:

A schematic representation of the steps followed for fabrication and characterization of flexible p-n junction diodes is shown in Fig. 5. Here, a thick p-type PEDOT:PSS was spin coated (~5 μm) on vertically aligned ZnO NRs/ZnO seed/Ni/substrates (Fig. 5b) and then, allowed it for three days in normal environment. Finally, a thin gold layer was coated at room temperature by e-beam evaporation with a thickness of 250 nm (Fig. 5c) and the I-V properties were measured at room

temperature. The fabricated p-n junction device exhibited excellent rectification diode characteristics even in fold condition, as shown in Fig. 6c. However, the amount of current flow through the device in fold condition is slightly lower than that of the flat condition. Under flat condition, the turn-on or knee-voltage of the device is about 3.37 V, whereas in fold state it slightly increased to 3.48 V. Upon folding, the series resistance of the device, evaluated from the slope of current-voltage (I-V) curves at above the knee-voltage, increased slightly from 53 to 65 kΩ. The probable reason for high turn-on voltage and series resistance could be due to the formation of strain in folded device. However, the overall changes in the properties of the device with folding are marginal. In reverse bias condition, the current flow through the device (leakage current) under both the conditions is low, which is in the order of 10^{-7} A. The rectification factor (on/off) of the device at bias voltage of 4 V is found to be ~153. These results are quite interesting than the devices fabricated with similar structures by Zainelabdin et al.[20] and Liu et al.[32]. This is probably attributed to the quality of present ZnO NRs.

To understand the current transport mechanism of the flexible device the experimental data (I-V) was fitted to an ideal diode equation (1) and quality factor (n) of the device was obtained using equation (2):[33]

$$I = I_o \left[\exp\left(\frac{qV}{nkT}\right) - 1\right] \quad (1)$$

and $$n = q\left[\left(\frac{\Delta \ln(I)}{\Delta V}\right) kT\right]^{-1} \quad (2).$$

Where I_o is the saturation current, q is the charge of electron, n is the diode quality factor (ideality factor), k is the Boltzmann's constant and T is the absolute temperature. ln(I) versus V plots (Fig. 7a) of the device measured under both the conditions exhibited three clearly distinguishable regions, treated as R-1, R-II and R-

III in forward bias region, 0 - +5 V, whereas in reverse bias condition (-5 – 0 V), it showed only two regions. Liu et al. also observed similar device behavior from annealed n-ZnO NRs/p-Si devices.[32] Under both the biasing conditions, the device behavior in R-I and R-II regions is comparable and similar. It indicates that the conduction mechanism of the device in R-I and R-II regions under both the biasing conditions could be same. However, a more precise analysis reveals that in reverse bias condition, the R-II region slightly lengthened up to the bias voltage of -5 V.

In order to understand detailed p-n junction behavior, the possible energy band alignment diagram of Ni/ZnO/PEDOT:PSS/Au device was constructed using Anderson Model, and is presented as Fig. 7b. Here, the electron affinity (χ) and band gap (E_g) of ZnO and PEDOT:PSS are considered as 4.2, 3.37, 3.6, and 1.6 eV and work function of Ni and Au are 5.3 and 5.1 eV, respectively. The band off-sets at conduction (ΔE_c) and valance (ΔE_v) bands of ZnO and PEDOT:PSS are calculated using the equations (3) and (4):

$$\Delta E_c = \chi(PEDOT{:}PSS) - \chi(ZnO) \quad (3)$$

$$\Delta E_v = E_g(ZnO) - E_g(PEDOT{:}PSS) - (\Delta E_c) \quad (4).$$

Fig. 7b shows that the fabricated device belongs to Type-II heterojunction (staggered) interface and consists of two different energy band off-sets (negative conduction off-set of 0.6 eV and positive valance band off-set of 1.17 eV) due to different electron affinities and energy band gaps of materials. Upon combining these two materials, the electrons accumulate at the interface of conduction bands due to the negative ΔE_c, whereas holes localize at the valance band of ZnO due to a large larger barrier with PEDOT:PSS. In forward bias condition (i.e. negative bias on n-ZnO), the current flow through the device mainly attributed to the conduction of holes from

PEDOT:PSS to ZnO (i.e. saturated current), whereas in reverse bias (positive bias on n-ZnO), the current flow majorly attributed to the conduction of electrons (i.e. rectification current). Thus, the device fabricated with ZnO NRs and PEDOT:PSS works as an reversed rectification diode to normal p-n junction diodes. Interestingly similar diode behavior has been observed by Bhat et al. from n-GaN/p-Si structures.[34]

From the functional fitting of ln(I) versus V plots, it is noticed that the current conduction of the device in R-I, R-II and R-III regions follows I α V (linear Ohmic), I α exp(c1V) (exponential growth) and I α V(c2+c3V) (combination of liner and square) relations, respectively. Here, the relational constants c1, c2 and c3 are found to be 1.42, 9.09 and -0.91, respectively, which can be clearly noticed from ln(I) versus ln(V) plots, as shown in Fig. 8. These analyses basically suggest that the transport mechanism of the device greatly depends on the bias voltage. The current conduction of the device at lower voltages (<1 V) is dominated by tunneling of thermally generated carriers or field emission mechanism,[35] whereas at higher voltages (>3 V) the device follows dual mechanisms such as tunneling and space-charge-limited current (SCLC) conduction. However, at moderate bias voltages (1 - 3 V) the conduction mechanism of the device follows recombination-tunneling mechanism.[32] Here, the observed exponential constant (c1) is low, thus the injection of carriers and thereby recombination of trap states is moderate. At higher voltages, the negative sign of c3 constant indicates that the influence of space charges on the current flow gradually increases with increase of bias voltage.

The diode quality factor of the device, calculated from ln(I) versus V plots, are presented in Figure 8. The ideality factor of the device in R-I region is about 1.44 eV,

which indicates that the behavior of flexible diode is nearly similar to an ideal diode and the transport mechanism of the device is field emission tunneling.[36] However, at higher biasing voltages, the ideality factor of the device is quite high (>10), probably due to the presence of native defect states on the surface of ZnO NRs,[37, 38] which probably act as additional current pathways through their energy levels.[39]

4. Conclusions

The impact of seed-layer deposition parameters like deposition potential and deposition time, and also annealing of seed-layers on the homo-epitaxial ZnO NRs morphology was investigated. Then, ZnO NRs grown under optimized conditions were adopted for the development of flexible devices and the performance of the devices was studied at room temperature. ZnO NRs grown on seed-layers deposited under a negative potential of 1.5 V in the duration of 2.5 min, followed by annealing at 200 ^{o}C for 2 h exhibited more uniform morphology, good chemical stoichiometry and single crystalline nature. The fabricated devices with high-quality ZnO NRs are highly flexible and exhibited excellent rectifying diode behavior. These devices showed nearly same diode performance even when they are in flat and fold conditions. From these results, therefore, it is emphasized that the methodology adopted for the development of high-quality ZnO NRs on flexible sheets as well as fabrication of flexible devices can be implemented for the realization of any devices (solar cells, sensors, bioelectronics and photonics) due to its simplicity, adoptability and quality along with cost less process.

Acknowledgement: N. K. Reddy wishes to acknowledge European Commission Research Executive Agency for the sanction of Marie Curie Actions - International

Incoming Fellowships (**No. PIIF-GA-2012-331003: NRforHF**). M. Devika wishes to acknowledge UGC for the sanction of Dr. D. S. Kothari Postdoctoral fellowship (**No. F.4-2/2006(BSR)/13-703/2012(BSR))**. This research was partly supported by the WCU (World Class University) program through the National Research Foundation of Korea funded by the Ministry of Education, Science and Technology (**R31-10026**).

Figure captions:

Fig. 1: FESEM images of ZnO NRs grown on seed-layers prepared by applying negative potential of (a) 1, (b) 1.5, (c) 2.0, and (d) 2.5 V for 1 min and annealed at a fixed temperature of 150 ^{o}C for 2 h.

Fig. 2: FESEM images of ZnO NRs grown on seed-layers prepared by applying negative potential of 1.5 V in the duration of (a) 30 s, (b) 1, (c) 2.5, and (d) 5 min and annealed at a fixed temperature of 150 ^{o}C for 2 h.

Fig. 3: FESEM images of ZnO NRs grown on seed-layers prepared by applying negative potential of 1.5 V for 2.5 min and annealed at (a) 100, (b) 150, (c) 200, and (d) 250 ^{o}C for 2 h.

Fig. 4: (a) TEM, (b) HRTEM, (c) SAED images of ZnO NRs grown on seed-layers prepared under optimized conditions (V_c = 1.5 V, D_t = 2.5 min, and A_T = 200 ^{o}C) and (d) its CL spectrum.

Fig. 5: Schematic representation of flexible p-n junction diode fabrication: (a) vertically aligned ZnO NRs on ZnO seed/Ni/Kapton substrate, (b) PEDOT:PSS spin

coated structures, (c) Au coated structures, and (d) contacts taken for I-V measurements.

Fig. 6: Photographs of flexible p-n junction diodes under (a) flat, (b) fold states, and (c) their corresponding current-voltage curves measured at room temperature.

Fig. 7: (a) ln(I) versus voltage plots of p-n junction diode measured at two different conditions and (b) the energy band diagram of Ni/ZnO/PEDOT:PSS/Au structure.

Fig. 8: ln(I) versus ln(V) plot of p-n junction diode measured at flat condition.

References:

1. D. Singh, A. A. Narasimulu, L. Garcia-Gancedo, Y. Q. Fu, N. Soin, G. Shao and J. K. Luo, *Nanotechnology*, 2013, **24**, 275601.
2. E. Monroy, F. Omnes and F. Calle, *Semicond Sci Tech*, 2003, **18**, R33-R51.
3. Z. Chen, N. Zhang and Y. J. Xu, *Crystengcomm*, 2013, 15, 3022-3030.
4. J. Liu, J. Goud, P. M. Raj, M. Iyer, Z. L. Wang and R. R. Tummala, *Elec Comp C*, 2008, 1317-1322.
5. L. Y. L. Wu, G. J. Loh, S. Fu, A. I. Y. Tok, X. T. Zeng, L. C. Kwek and F. C. Y. Boey, *Mater Res Soc Symp P*, 2009, **1191**, 121-126.
6. Y. L. Wu, C. S. Lim, S. Fu, A. I. Y. Tok, H. M. Lau, F. Y. C. Boey and X. T. Zeng, *Nanotechnology*, 2007, **18**.
7. B. Weng, S. Q. Liu, Z. R. Tang and Y. J. Xu, *Rsc Adv*, 2014, 4, 12685-12700.
8. D. K. Hwang, M. S. Oh, J. H. Lim and S. J. Park, *J Phys D Appl Phys*, 2007, **40**, R387-R412.
9. U. Ozgur, D. Hofstetter and H. Morkoc, *P Ieee*, 2010, **98**, 1255-1268.
10. U. Ozgur, Y. I. Alivov, C. Liu, A. Teke, M. A. Reshchikov, S. Dogan, V. Avrutin, S. J. Cho and H. Morkoc, *J Appl Phys*, 2005, **98**.
11. H. J. Zhou and S. S. Wong, *Acs Nano*, 2008, **2**, 944-958.
12. P. X. Gao, J. H. Song, J. Liu and Z. L. Wang, *Adv Mater*, 2007, **19**, 67-+.
13. X. Y. Pan, M. Q. Yang and Y. J. Xu, *Phys Chem Chem Phys*, 2014, 16, 5589-5599.
14. K. Zhang, J. H. Seo, W. D. Zhou and Z. Q. Ma, *Journal of Physics D-Applied Physics*, 2012, **45**.
15. T. Y. Liu, H. C. Liao, C. C. Lin, S. H. Hu and S. Y. Chen, *Langmuir*, 2006, **22**, 5804-5809.
16. L. Huang, G. L. Guo, Y. Liu, Q. H. Chang and W. Z. Shi, *Mater Res Bull*, 2013, **48**, 4163-4167.

17. S. Park, J. H. Lee, H. D. Kim, S. M. Hong, H. M. An and T. G. Kim, *Phys Status Solidi-R*, 2013, **7**, 493-496.
18. A. Rivera, A. Edington, J. Zeller and M. Anwar, *P Ieee Les Eastm*, 2012.
19. Y. Qiu, H. Q. Zhang, L. Z. Hu, D. C. Yang, L. N. Wang, B. Wang, J. Y. Ji, G. Q. Liu, X. Liu, J. F. Lin, F. Li and S. J. Han, *Nanoscale*, 2012, **4**, 6568-6573.
20. A. Zainelabdin, S. Zaman, G. Amin, O. Nur and M. Willander, *Nanoscale Res Lett*, 2010, **5**, 1442-1448.
21. K. H. Lee, B. Kumar, H. J. Park and S. W. Kim, *Nanoscale Research Letters*, 2010, **5**, 1908-1912.
22. C. T. Hsieh, J. Y. Lin and S. Y. Yang, *Physica E*, 2010, **42**, 2319-2323.
23. C. C. Lin, H. P. Chen, H. C. Liao and S. Y. Chen, *Appl Phys Lett*, 2005, **86**.
24. A. Manekkathodi, M. Y. Lu, C. W. Wang and L. J. Chen, *Adv Mater*, 2010, **22**, 4059-4063.
25. J. J. Kim, K. S. Kim and G. Y. Jung, *J Mater Chem*, 2011, **21**, 7730-7735.
26. C. Y. Lee, M. Y. Lin, W. H. Wu, J. Y. Wang, Y. Chou, W. F. Su, Y. F. Chen and C. F. Lin, *Semicond Sci Tech*, 2010, **25**.
27. N. Koteeswara Reddy, M. Devika and C. W. Tu, *Materials Letters*, 2014, **120**, 62-64.
28. A. Kathalingam, M. R. Kim, Y. S. Chae, J. K. Rhee and T. Mahalingam, *J Korean Phys Soc*, 2009, **55**, 2476-2481.
29. S. X. Dai, Y. Y. Li, Z. L. Du and K. R. Carter, *J Electrochem Soc*, 2013, **160**, D156-D162.
30. N. K. Reddy, M. Devika, N. Shpaisman, M. Ben-Ishai and F. Patolsky, *J Mater Chem*, 2011, **21**, 3858-3864.
31. A. B. Djurisic and Y. H. Leung, *Small*, 2006, **2**, 944-961.
32. S. Y. Liu, T. Chen, Y. L. Jiang, G. P. Ru and X. P. Qu, *Journal of Applied Physics*, 2009, **105**.
33. [12]. Sze S M Semiconductor Devices Physics and Technology, New Jersey: John Wiley & Sons, 1985.
34. T. N. Bhat, M. K. Rajpalke, B. Roul, M. Kumar and S. B. Krupanidhi, *J Appl Phys*, 2011, **110**.
35. N. K. Reddy, Q. Ahsanulhaq, J. H. Kim and Y. B. Hahn, *Appl Phys Lett*, 2008, **92**.
36. C. T. Sah, R. N. Noyce and W. Shockley, *P Ire*, 1957, **45**, 1228-1243.
37. P. Deb, H. Kim, Y. X. Qin, R. Lahiji, M. Oliver, R. Reifenberger and T. Sands, *Nano letters*, 2006, **6**, 2893-2898.
38. A. Motayed, A. V. Davydov, M. D. Vaudin, I. Levin, J. Melngailis and S. N. Mohammad, *J Appl Phys*, 2006, **100**.
39. N. Bano, S. Zaman, A. Zainelabdin, S. Hussain, I. Hussain, O. Nur and M. Willander, *J Appl Phys*, 2010, **108**.

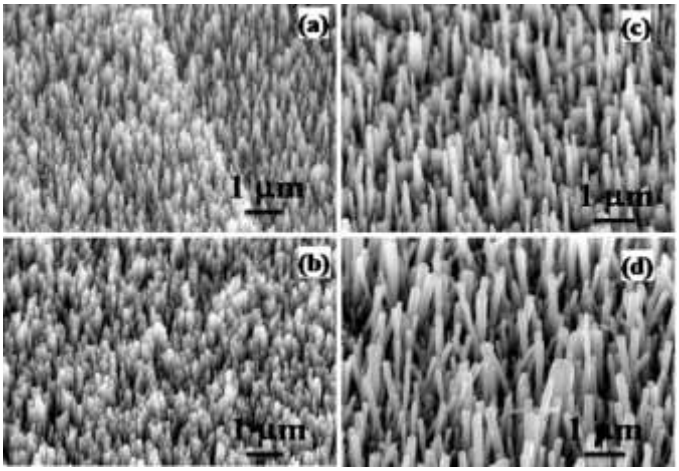

Fig. 1

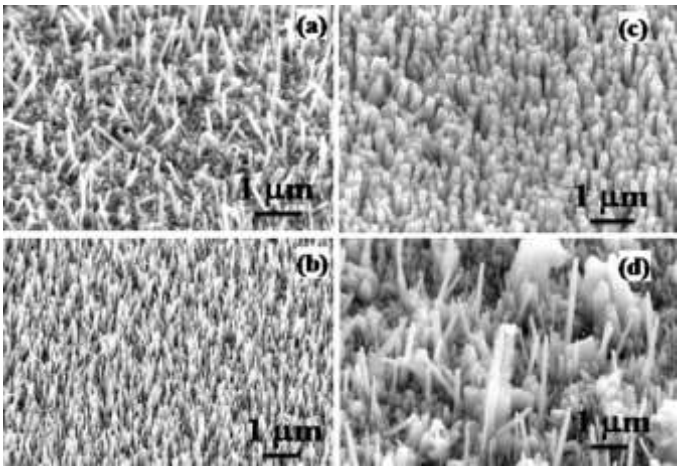

Figure 2

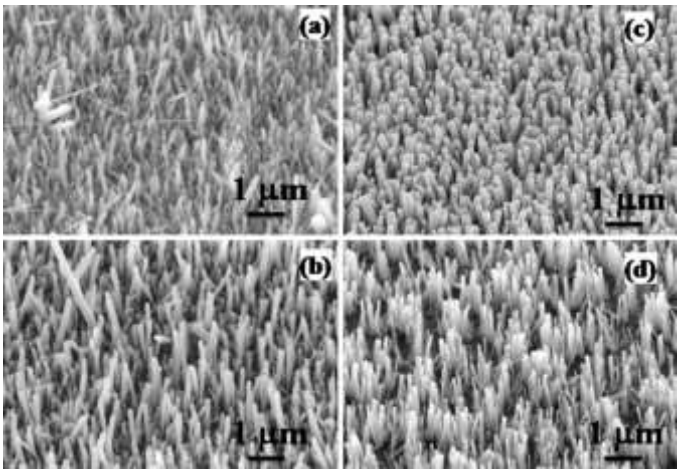

Fig. 3

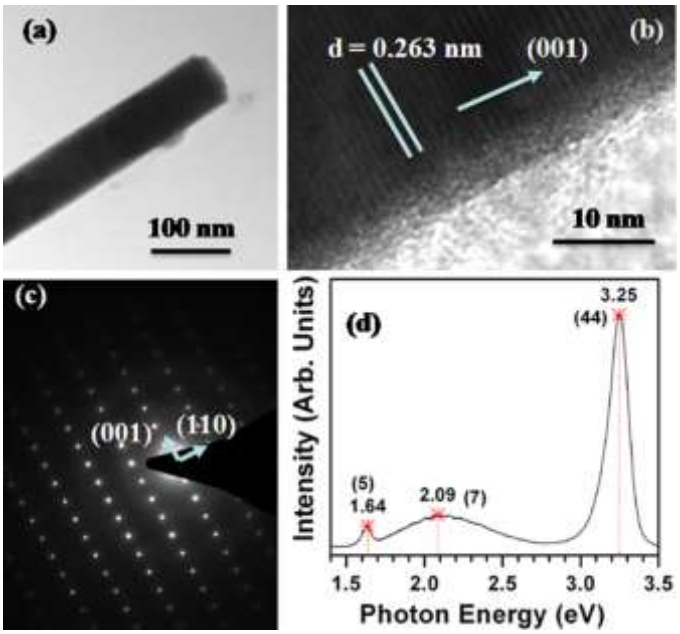

Fig. 4

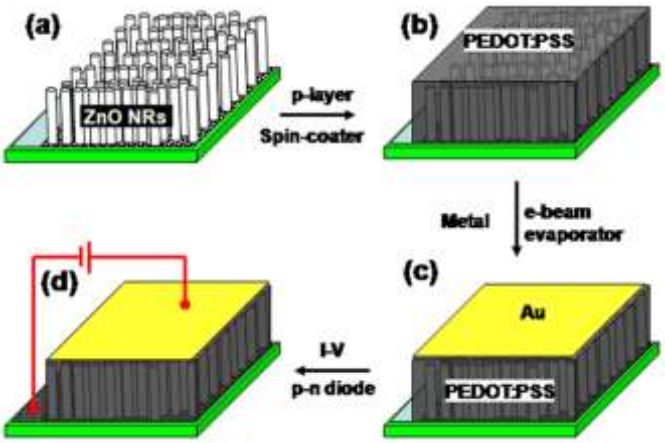

Fig. 5

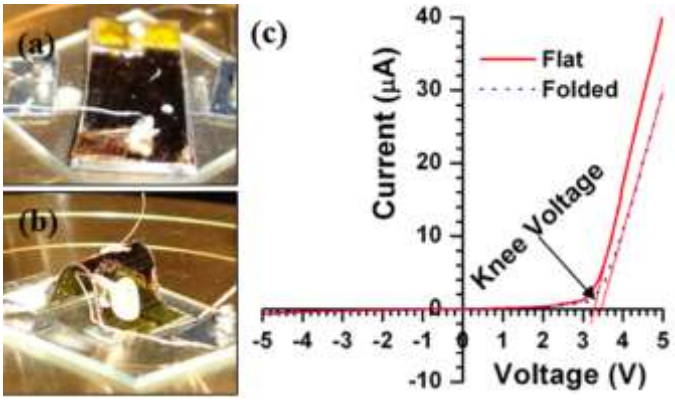

Fig. 6

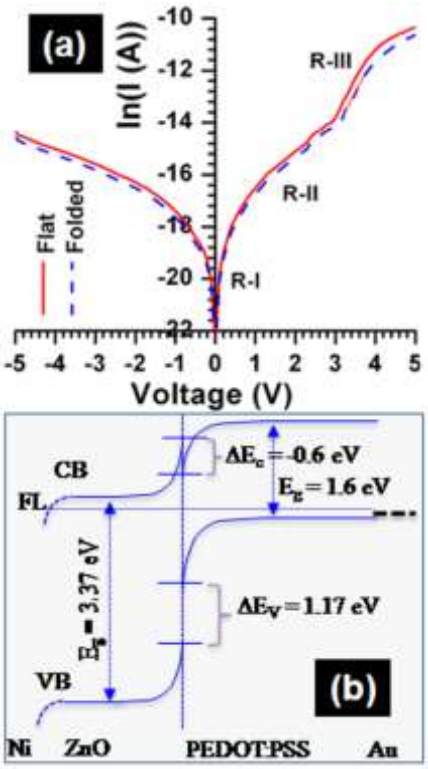

Fig. 7

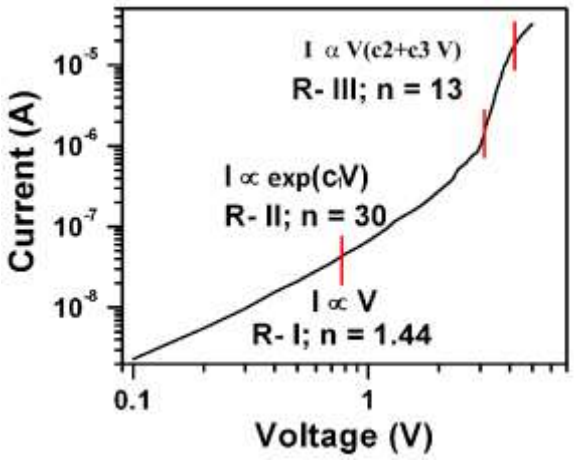

Fig. 8